Single Crystalline Alkaline-Earth Metal Hexaboride One-Dimensional (1D) Nanostructures: Synthesis and Characterization

Syed S. Amin,[†] Shu-you Li,[‡] John R. Roth,[§] and Terry T. Xu*,[†]

Department of Mechanical Engineering and Engineering Science, The University of North Carolina at Charlotte, Charlotte, North Carolina 28223, NUANCE center, Northwestern University, Evanston, Illinois 60208, and Research Resource Center, University of Illinois at Chicago, Chicago, Illinois 60612

Received July 23, 2008. Revised Manuscript Received December 23, 2008

Catalytic material-assisted growth of alkaline-earth metal hexaboride (MB_6, M = Sr, Ba) 1D nanostructures was achieved by pyrolysis of diborane (B_2H_6) over alkaline-earth metal oxide (MO) powders at elevated temperature (~840−870 °C) and low pressure (~165 mTorr). The as-synthesized MB_6 1D nanostructures were characterized by scanning electron microscopy (SEM), transmission electron microscopy (TEM), and Raman spectroscopy. Results show that the MB_6 nanostructures are single crystalline with the preferred growth direction along [001]. The SrB_6 nanowires are ~20−100 nm in diameter and ~2−5 μm in length. The BaB_6 nanostructures have a rectangular cross section (width ~20−300 nm) and are ~5−20 μm in length. The growth of these MB_6 nanostructures can be attributed to a nontraditional vapor−solid−liquid (VLS)-like growth mechanism. The as-synthesized MB_6 1D nanostructures are promising *n*-type low-dimensional thermoelectric materials.

Introduction

The divalent alkaline-earth metal hexaborides (CaB_6, SrB_6, and BaB_6) are known for their low densities, high melting points, high hardness, high Young's moduli, low thermal expansion coefficients, and high chemical stability.[1,2] They have found applications, for example, in high temperature insulation and nuclear engineering and as cathode materials.[1,2] Recently, these hexaborides have received considerable attention because of their controversial weak ferromagnetism,[3−5] debatable electronic structures,[6,7] promising thermoelectric properties,[8,9] and others.[10,11]

One of the potential applications of alkaline-earth metal hexaborides is to serve as *n*-type thermoelectric materials for high temperature power generation.[8,9] Although some boron-rich materials (e.g., β-rhombohedral boron, AlB_{12}, $B_{13}C_2$, and $B_{14}Si$) have been revealed as good *p*-type thermoelectric materials,[12] there has been a lack of development in synthesis and understanding of *n*-type boron-rich thermoelectric materials. Recent theoretical and experimental work demonstrated that alkaline-earth metal hexaborides are promising *n*-type thermoelectric materials with large Seebeck coefficients (S) and high electrical conductivities (σ).[8,9,13,14] In particular, (i) the thermoelectric figure of merit (ZT) of SrB_6 was measured to be approximately 0.3 at 1073 K;[14] (ii) the high value (higher than that of boron carbide) and temperature independent characteristic of the power factor (defined as $S^2\sigma$) were observed for CaB_6 and SrB_6;[13] and (iii) alloying was found to be an effective way to improve the thermoelectric performance (e.g., ZT of $Ca_{0.5}Sr_{0.5}B_6$ reached 0.35 at 1073 K).[9]

Although promising thermoelectric properties were observed from alkaline-earth metal hexaborides, improved thermoelectric performance (i.e., higher ZT) is inevitably needed to facilitate the realization of future high-efficient thermoelectric devices. It is of recent advances that low-dimensional materials such as quantum dots, nanowires, and thin films provide new opportunities to achieve higher ZT.[15−17] Because of both a higher density of states induced

* To whom all correspondence should be addressed. Telephone: (704) 687-8353. Fax: (704) 687-8345. E-mail: ttxu@uncc.edu.
[†] The University of North Carolina at Charlotte.
[‡] Northwestern University.
[§] University of Illinois at Chicago.

(1) Adams, R. M. *Boron, Metallo-Boron Compounds, and Boranes*; Interscience Pulishers: New York, 1964.
(2) Matkovich, V. I. *Boron and Refractory Borides*; Springer-Verlag: Berlin, 1977.
(3) Ott, H. R.; Gavilano, J. L.; Ambrosini, B.; Vonlanthen, P.; Felder, E.; Degiorgi, L.; Young, D. P.; Fisk, Z.; Zysler, R. *Physica B* **2000**, *281*, 423.
(4) Young, D. P.; Hall, D.; Torelli, M. E.; Fisk, Z.; Sarrao, J. L.; Thompson, J. D.; Ott, H. R.; Oseroff, S. B.; Goodrich, R. G.; Zysler, R. *Nature* **1999**, *397*, 412.
(5) Dorneles, L. S.; Venkatesan, M.; Moliner, M.; Lunney, J. G.; Coey, J. M. D. *Appl. Phys. Lett.* **2004**, *85*, 6377.
(6) Massidda, S.; Continenza, A.; dePascale, T. M.; Monnier, R. *Z. Phys. B: Condens. Matter.* **1997**, *102*, 83.
(7) Ott, H. R.; Chernikov, M.; Felder, E.; Degiorgi, L.; Moshopoulou, E. G.; Sarrao, J. L.; Fisk, Z. *Z. Phys. B: Condens. Matter.* **1997**, *102*, 337.
(8) Imai, Y.; Mukaida, M.; Ueda, M.; Watanabe, A. *Intermetallics* **2001**, *9*, 721.
(9) Takeda, M.; Terui, M.; Takahashi, N.; Ueda, N. *J. Solid State Chem.* **2006**, *179*, 2823.
(10) Shang, S.; Wang, Y.; Liu, Z.-K. *Phys. Rev. B* **2007**, *75*, 024302/1.
(11) Shang, S.; Liu, Z.-K. *Appl. Phys. Lett.* **2007**, *90*, 091914/1.
(12) Wood, C. *Rep. Prog. Phys.* **1988**, *51*, 459.
(13) Takeda, M.; Fukuda, T.; Domingo, F.; Miura, T. *J. Solid State Chem.* **2004**, *177*, 471.
(14) Takeda, M.; Fukuda, T.; Miura, T. *Proceedings of 21st International Conference on Thermoelectrics*; IEEE: Piscataway, NJ, 2002; p 173.
(15) Dresselhaus, M. S.; Dresselhaus, G.; Sun, X.; Zhang, Z.; Cronin, S. B.; Koga, T. *Phys. Solid State* **1999**, *41*, 679.

10.1021/cm802018e CCC: $40.75
Published on Web 01/27/2009

by quantum confinement effects for enhanced Seebeck coefficient and increased phonon boundary or interface scattering for reduced thermal conductivity, enhanced thermoelectric performance in low-dimensional materials as compared to their counterpart bulk materials can be realized.[15,16] Thus, it is of interest to synthesize low-dimensional alkaline-earth metal hexaborides and explore whether they exhibit better thermoelectric performance. As the first step of our ongoing project, successful synthesis and understanding of the growth mechanisms of the low-dimensional alkaline-earth metal hexaborides are critical. Our current focus is on one-dimensional (1D) nanostructures.

There have been several recent reports on synthesis and characterization of 1D metal hexaboride nanostructures, especially on rare earth metal hexaborides due to their promising field emission properties.[18−24] However, for 1D alkaline-earth metal hexaborides, only CaB_6 1D nanostructures were recently synthesized by both catalytic materials-assisted vapor−liquid−solid (VLS)[25] and self-catalytic vapor−solid (VS) growth.[26] There has been no description on synthesis of SrB_6 and BaB_6 1D nanostructures. In this paper, we report the catalytic materials-assisted growth of MB_6 (M = Sr, Ba and hereafter) 1D nanostructures by pyrolysis of diborane (B_2H_6) over respective MO powders at 840−870 °C and ∼165 mTorr. Nickel is the most effective catalytic material. The as-synthesized SrB_6 nanostructures are ∼20−100 nm in diameter and ∼2−5 μm in length. The BaB_6 nanostructures have a rectangular cross section (width ∼20−300 nm) and are ∼5−20 μm in length. The MB_6 1D nanostructures are single crystalline with the growth direction along [001] direction. Different from the reported VLS and self-catalytic VS growth of CaB_6 1D nanostructures, a unique nontraditional VLS-like growth mechanism is identified for growth of SrB_6 and BaB_6 1D nanostructures reported in this study.

Experimental Section

The experiments were carried out in a low pressure chemical vapor deposition (LPCVD) system similar to the one described in ref 27, with the modification of replacement of the convection pressure gauge with a wide-range diaphragm manometer (Kurt J Lesker: KJLC 1500WR series) to provide more accurate pressure measurement. To prevent the possible hazard (e.g., toxic by inhalation, flammable) caused by B_2H_6, the gas cylinder is stored in a gas cabinet, and the majority parts of the LPCVD are located within a fume hood.

Silicon (Si) wafers with one-micrometer-thick thermally grown silicon dioxide: SiO_2 (University Wafer) were cut into small pieces with the specific size of 5 mm (width) × 20 mm (length). These SiO_2−Si substrates were ultrasonically cleaned using acetone and methanol (Branson Ultrasonic Cleaner; 3 min) followed by oxygen plasma cleaning (Kurt J Lesker: Plasma-Preen 862; 3 min). Respective oxide powders (SrO, Sigma Aldrich, 99.9% purity; BaO, Sigma Aldrich, 99.99% purity) were then randomly dispersed on SiO_2−Si substrates by a dry transfer method, followed by the deposition of a thin nickel (Ni) film (2−8 nm) using a magnetron sputter (Denton Vacuum: Desk IV TSC). The specific Ni/MO/SiO_2−Si substrates were loaded into a quartz boat and placed in a desired position in the 1 in. diameter quartz tube reaction chamber of the LPCVD system. The whole system was evacuated to a pressure of ∼5 mTorr. For growth of MB_6 1D nanostructures, the chamber temperature (temperature was measured at the center of the reaction chamber) was ramped up to 950 °C in 60 min with constant flow of 10 sccm (standard cubic centimeter per minute) Ar (Linde; 99.999% UHP) as the carrier gas and soaked at that temperature for 30 min during which 10 sccm B_2H_6 (Voltaix; 5% UHP diborane in research grade Ar) was introduced along with the carrier gas. The reaction pressure for each run was maintained at ∼165 mTorr. After reaction, the chamber was cooled to room temperature in ∼5 h under 10 sccm Ar flow. The substrates were then taken out for characterization.

The as-synthesized samples were characterized by scanning electron microscopy (SEM; JEOL JSM-6480), transmission electron microscopy (TEM; JEOL JEM-2100F with Low-Z (Be) sample holder for analytical X-ray microanalysis) including electron diffraction, high-resolution TEM (HRTEM), energy dispersive X-ray spectroscopy (EDX; with ultra-thin window X-ray detector which is capable of detecting boron), and electron energy loss spectroscopy (EELS). Micro-Raman spectroscopy (Renishaw RM 2000 confocal micro-Raman system in the back-scattering configuration; 514.5 nm excitation green laser) was also performed.

Results

SEM images showing typical morphologies of as-synthesized 1D nanostructures on Ni/MO/SiO_2−Si substrates are presented in Figure 1. Figure 1a−c shows 1D nanostructures on a Ni/SrO/SiO_2−Si substrate. These nanostructures were found on the substrate placed in the 840−870 °C temperature zone of the reaction chamber. Figure 1a is a low magnification image, showing several fluffy white powders on the substrate. A closer view reveals numerous 1D nanostructures grown on both the powders (Figure 1b) and the substrate areas surrounding them (the enclosed white square in Figure 1a is enlarged and shown as Figure 1c). However, more 1D nanostructures can be identified on the powders. Most of the 1D nanostructures are tapered, with a diameter ranging from approximately 80−100 nm at the root and 20−30 nm at the tip. The nanostructures are roughly 2−5 μm in length. No obvious Ni particles can be observed from the tips of the as-synthesized nanostructures. However, EDX mapping (results not shown here) showed that Ni

(16) Chen, G.; Dresselhaus, M. S.; Dresselhaus, G.; Fleurial, J. P.; Caillat, T. *Int. Mater. Rev.* **2003**, *48*, 45.
(17) Dresselhaus, M. S.; Chen, G.; Tang, M. Y.; Yang, R. G.; Lee, H.; Wang, D. Z.; Ren, Z. F.; Fleurial, J. P.; Gogna, P. *Adv. Mater.* **2007**, *19*, 1043.
(18) Zhang, H.; Zhang, Q.; Tang, I.; Qin, L. C. *J. Am. Chem. Soc.* **2005**, *127*, 8002.
(19) Zhang, H.; Zhang, Q.; Tang, I.; Qin, L. C. *J. Am. Chem. Soc.* **2005**, *127*, 2862.
(20) Zhang, H.; Zhang, Q.; Zhao, G. P.; Tang, J.; Zhou, O.; Qin, L. C. *J. Am. Chem. Soc.* **2005**, *127*, 13120.
(21) Brewer, J. R.; Deo, N.; Wang, Y. M.; Cheung, C. L. *Chem. Mater.* **2007**, *19*, 6379.
(22) Ding, Q. W.; Zhao, Y. M.; Xu, J. Q.; Zou, C. Y. *Solid State Commun.* **2007**, *141*, 53.
(23) Xu, J. Q.; Chen, X. L.; Zhao, Y. M.; Zou, C. Y.; Ding, Q. W.; Jian, J. K. *J. Cryst. Growth* **2007**, *303*, 466.
(24) Xu, J. Q.; Chen, X. L.; Zhao, Y. M.; Zou, C. Y.; Ding, Q. W. *Nanotechnology* **2007**, 18.
(25) Xu, T. T.; Zheng, J. G.; Nicholls, A. W.; Stankovich, S.; Piner, R. D.; Ruoff, R. S. *Nano Lett.* **2004**, *4*, 2051.
(26) Xu, J. Q.; Zhao, Y. M.; Zou, C. Y.; Ding, Q. W. *J. Solid State Chem.* **2007**, *180*, 2577.
(27) Xu, T. T.; Zheng, J. G.; Wu, N. Q.; Nicholls, A. W.; Roth, J. R.; Dikin, D. A.; Ruoff, R. S. *Nano Lett.* **2004**, *4*, 963.

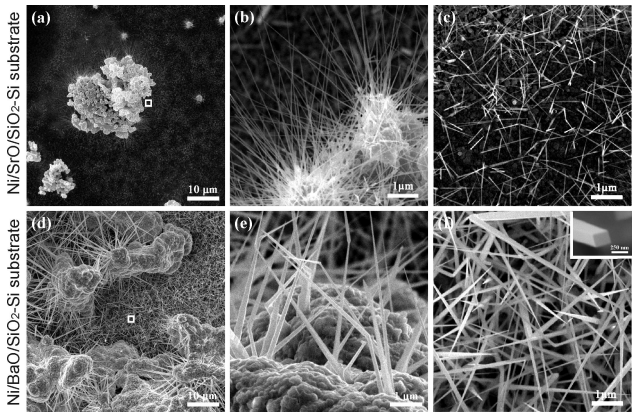

Figure 1. SEM micrographs of as-synthesized 1D nanostructures on Ni/SrO/SiO_2−Si (a, b, c) and Ni/BaO/SiO_2−Si (d, e, f) substrates. Tapered 1D nanostructures can be observed from both MO powders and substrate areas surrounding the powders (enclosed by white squares in a and d). On the Ni/SrO/SiO_2−Si substrate, SrO powders are favorable sites where 1D nanostructures were grown. On the Ni/BaO/SiO_2−Si substrate, substrate areas surrounding BaO powders are preferred regions where 1D nanostructures were grown. The scale bar of the inset in part f represents 250 nm.

distributed randomly over the whole substrate. Figure 1d−f shows the 1D nanostructures on a Ni/BaO/SiO_2−Si substrate. These nanostructures were found on the substrate placed in the 860−870 °C temperature zone of the reaction chamber. Again, 1D nanostructures can be seen from both the powders (Figure 1e) and the substrate areas surrounding them (Figure 1f). However, in contrast to those observed on Ni/SrO/SiO_2−Si substrates, more 1D nanostructures can be observed from the substrate areas on Ni/BaO/SiO_2−Si substrates. The tapered and sometimes kinked 5−20 μm long 1D nanostructures have rectangular cross sections (see the inset of Figure 1f) with width ranging from ∼20−300 nm.

Figure 2 presents the micro-Raman spectra of as-synthesized 1D nanostructures acquired at room temperature in ambient atmosphere. For 1D nanostructures grown on Ni/SrO/SiO_2−Si substrates, the peaks at 771, 1086, and 1232 cm^{-1} match the reported experimental[28,29] and calculated[10,28] values for Raman active modes A_{1g}, E_g, and T_{2g}, respectively, of SrB_6. For 1D nanostructures grown on Ni/BaO/SiO_2−Si substrates, the peaks at 736, 989, and 1115 cm^{-1} are close to the published calculated values of BaB_6.[10] For further confirmation, micro-Raman spectroscopy was performed on commercial SrB_6 and BaB_6 powders (Alfa Aesar; >99% purity). Results verified the as-synthesized 1D nanostructures are MB_6 materials. The shift and broadening of Raman peaks of the MB_6 1D nanostructures from those of commercial powders might be attributed to the changes of local structure of boron octahedra due to impurities[30] and others.[31,32]

To obtain detailed information regarding to the crystallinity, morphology, chemical composition, and growth direc-

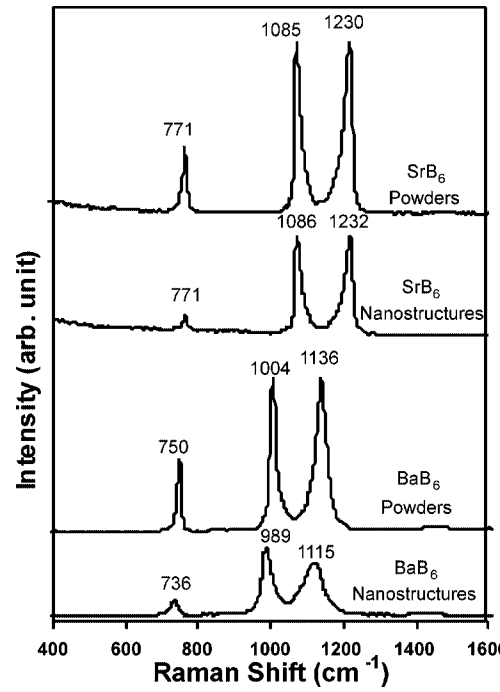

Figure 2. Micro-Raman spectra of as-synthesized 1D nanostructures and commercial MB_6 powders. The three peaks at progressively higher shift (cm^{-1}) correspond to A_{1g}, E_g, and T_{2g} active Raman modes, respectively, of MB_6. Results verified the as-synthesized 1D nanostructures are MB_6 materials.

tion of as-synthesized 1D nanostructures, TEM/EDX/electron diffraction pattern analyses were performed on approximately 20 nanowires, and representative results are discussed as follows. Figure 3a is a low magnification TEM image, showing a portion of a nanostructure obtained from a Ni/SrO/SiO_2−Si substrate. There is no catalytic material observed on the tip of the nanostructure. Figure 3b is a HRTEM image of the section enclosed by the black square in Figure 3a, illustrating the nanostructure has a single-crystalline core and a 1−2 nm thick amorphous sheath. The inset in Figure 3b is the corresponding diffraction pattern recorded in [$\bar{1}$00] axis. On the basis of the HRTEM imaging and electron diffraction pattern analysis, the lattice constant of the nanostructure is calculated as $a = 0.418 \pm 0.001$ nm, which is close to that of cubic SrB_6 from the JCPDS database (no. 28-1210, $a = 0.4193$ nm). The growth direction of the nanostructure is determined to be the [001] direction. EDX (STEM mode; 1 nm probe size) was used to study the chemical composition of the core and amorphous sheath, respectively, of the nanostructure. The representative EDX spectra shown in Figure 3c reveal the existence of Sr, B, O, and possible Si in both the core and the sheath (Note: the Cu signal comes from the supporting Cu grid and is not a component of the nanostructure). The higher O:B ratio observed from the sheath (see the inset of Figure 3c) indicates the periphery of the nanostructure is rich in O. Thus, based on TEM/EDX/electron diffraction pattern analyses, the nanostructure is determined to have a single crystalline SrB_6 core covered by a thin amorphous sheath containing Sr, O, and possible B. A very small amount of Si exists in both the core and the sheath. The source of Si was discussed in our previous publication.[33] In general, the Si might come from the SiO_2−Si substrates, quartz boats, and quartz tubes

(28) Yahia, Z.; Turrell, S.; Turrell, G.; Mercurio, J. P. *J. Mol. Struct.* **1990**, *224*, 303.
(29) Yahia, Z.; Turrell, S.; Mercurio, J. P.; Turrell, G. *J. Raman Spectrosc.* **1993**, *24*, 207.
(30) Song, M.; Yang, I. S.; Kim, J. Y.; Cho, B. K. *Vib. Spectrosc.* **2006**, *42*, 288.
(31) Campbell, I. H.; Fauchet, P. M. *Solid State Commun.* **1986**, *58*, 739.
(32) Richter, H.; Wang, Z. P.; Ley, L. *Solid State Commun.* **1981**, *39*, 625.

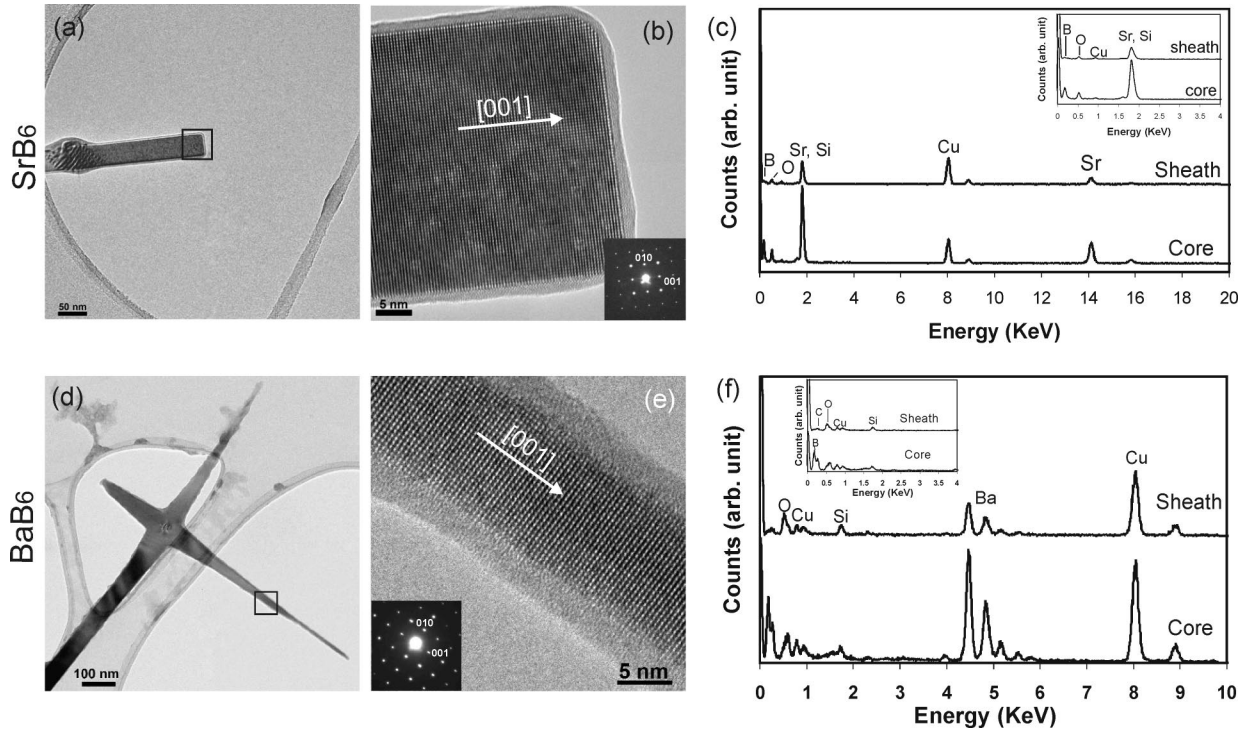

Figure 3. TEM/EDX/electron diffraction pattern analyses of typical 1D nanostructures grown on Ni/SrO/SiO_2−Si (a, b, c) and Ni/BaO/SiO_2−Si (d, e, f) substrates. The nanostructures are single crystalline MB_6 1D nanostructures, covered by amorphous oxide thin sheathes. No catalytic materials can be identified from the tips of nanostructures.

used for the experiments. The Si impurity might be one reason which causes the shift of Raman peaks shown in Figure 2.

Similar TEM/EDX/electron diffraction pattern results were obtained from 1D nanostructures grown on Ni/BaO/SiO_2−Si substrates. Figure 3d−f illustrates one typical 1D nanostructure that has a single crystalline BaB_6 core grown in the [001] direction. The crystallized core is covered by a thin amorphous sheath containing Ba, O, and possible B. Silicon is the impurity observed in both the core and the sheath. As discussed later in the text, the observed C peaks in EDX spectra are related to the adsorption of C-containing molecules after exposing the sample to the ambient environment. Again, no catalytic material can be observed from the tips of the nanostructure.

In summary, the as-synthesized 1D nanostructures on Ni/MO/SiO_2−Si substrates were characterized to be MB_6 materials. The MB_6 1D nanostructures have single crystalline MB_6 cores and 1−2 nm wide amorphous MO sheathes. Although Ni was used as the catalytic material during syntheses, it was not detected at the tips of as-synthesized 1D nanostructures.

Discussion

To explore the growth mechanisms of as-synthesized MB_6 1D nanostructures, a series of systematic experiments were carried out to study the effects of solid precursor MO powders, catalytic materials, substrates, reaction temperatures, and reaction duration. A nontraditional VLS-like growth mechanism is proposed based on the experimental results.

1. Heating of Bare MO or Ni-Coated MO Powders in an Ar Environment—Evidence of Melting at Elevated Temperatures. Controlled experiments of direct heating of (i) bare MO and (ii) Ni-coated MO powders on SiO_2−Si substrates at elevated temperatures (950 °C) in an Ar environment were carried out. Growth of 1D nanostructures was not observed. However, evidence of melting of powders at the reaction temperatures was revealed. Both MO and Ni-coated MO powders exhibited clear morphological changes before and after heating. For Ni-coated MO powders, isolated Ni islands were also observed after heating.

Figure 4a shows the morphology of Ni-coated SrO powders on a SiO_2−Si substrate before heating. On the substrate, no special features along the peripheries of powders can be observed. Figure 4b presents the morphology of Ni-coated SrO powders on a SiO_2−Si substrate after heating. On the substrate, light gray peripheries surrounding powders (so-called "molten peripheries"; indicated by white arrows) can be observed. The inset is a high-magnification SEM image, clearly showing the "molten peripheries" surrounding SrO powders. EDX analyses were performed on the powders, "molten peripheries", and substrate to disclose their compositional difference. As shown in Figure 4c, the existence of Sr, O, Si, and Ni is revealed from both the powders and the "molten peripheries"; whereas only O, Si, and Ni can be detected from the substrate. The SEM/EDX analyses indicate that part of SrO powders might go through a melt−solidification process during the experiments.

Evidence of melting at the reaction temperatures was also observed from Ni-coated BaO powders (Figure 4d−f). Figure 4e shows the morphology of BaO powders after heating, from which "molten peripheries" surrounding the powders

(33) Xu, T. T.; Nicholls, A. W.; Ruoff, R. S. *Nano* **2006**, *1*, 55.

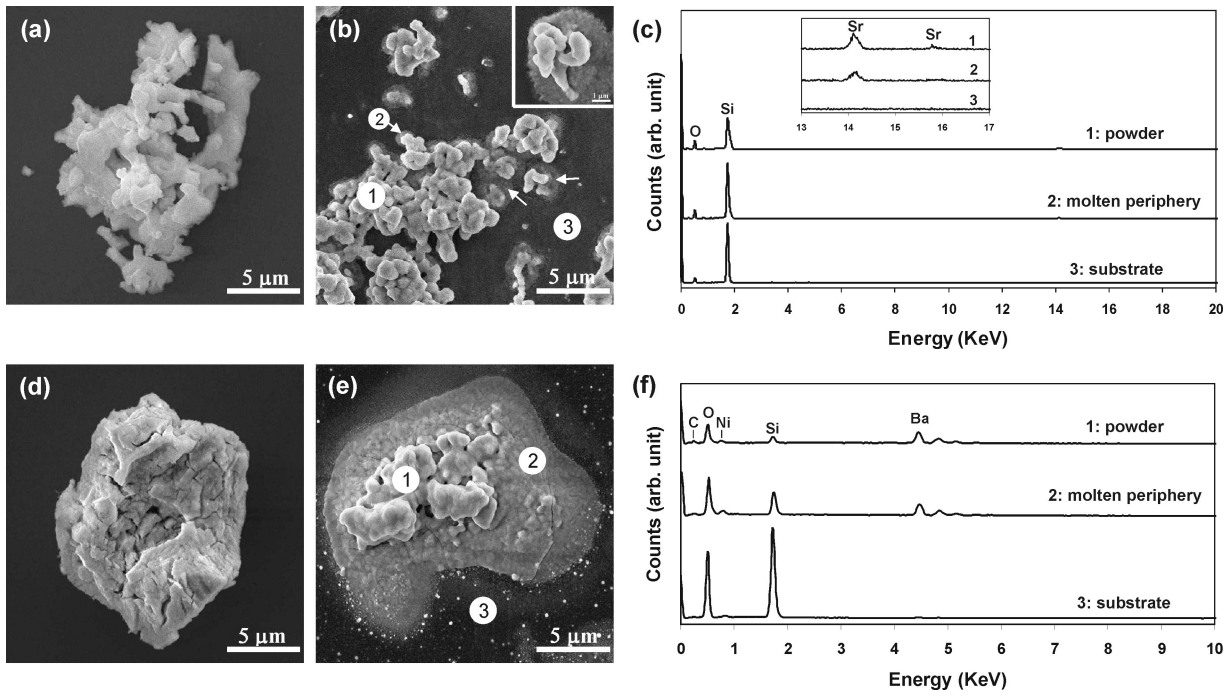

Figure 4. SEM/EDX examination of SrO (a−c) and BaO (d−e) powders before (a, d) and after (b, c, e, f) heating in an Ar environment at elevated temperatures. Melting of the powders is evident. The scale bar for the inset in part b is 1 μm.

can be easily identified. These "molten peripheries" are more obvious compared to those surrounding SrO powders (Figure 4b). From some samples, dendritic structures could be observed, strongly implying the occurrence of a melt−solidification process happened during the experiments.

So far, the real scenario on how the melt−solidification process occurred is not clear. However, it is possible that (1) at elevated temperatures, the surfaces of MO powders were in the molten state. Flow of the superficial liquid MO might also occur, resulting in the formation of "molten peripheries" surrounding the powders on the substrate; and/or (2) at the interface between MO and SiO_2−Si substrate, a solid state reaction might happen to form alkaline-earth metal silicates ($M_xSi_yO_z$)[34] which were likely in a molten state at the reaction temperature. Flow of silicates could happen, resulting in the formation of "molten peripheries". Regardless of their causes, the "molten peripheries" are believed to be the preferred sites for adsorbing borane molecules and facilitating the growth of MB_6 1D nanostructures (as discussed later in the text). To investigate which aforementioned possibility could be more feasible, annealing of MO powders was done on sapphire substrates with 5 μm thick GaN film on top (GaN-Al_2O_3). The GaN-Al_2O_3 substrate was chosen because no possible solid state reactions between GaN and MO could be identified by literature search. On annealed MO/GaN-Al_2O_3 substrates, "molten peripheries" were again seen around MO powders. This result indicates that surface melting of MO powders could be dominating at elevated temperatures.

Although the melting temperatures of bulk MO materials (2430 °C for SrO; 1920 °C for BaO)[35] are much higher than the reaction temperature used in this study (950 °C), the melting of submicrometer size MO powders is in evidence. This observation is consistent with reported phenomena that the melting temperature of a solid particle or small cluster decreases with the decreasing of its size.[36] For example, the surface melting of Pt nanocrystals was observed at ∼500 °C, which is much lower than the melting temperature of bulk Pt (1769 °C).[37] In the present study, the more evident melting of BaO powders (Figure 4e) than that of SrO powders (Figure 4b) at the same reaction temperature can be attributed to the lower melting point of bulk BaO than that of SrO.

In addition to the "molten peripheries", isolated Ni islands were observed on the Ni/MO/SiO_2−Si substrates after heating. Isolated Ni islands were also the characteristic features on annealed Ni/SiO_2−Si substrates. Although the formation mechanism of these Ni islands might be attributed to a dewetting−agglomeration behavior[38,39] of the 2 nm Ni thin film, the status of them (i.e., solid or liquid; solubility with MO liquid) at the reaction temperatures is not clear. However, it is believed that these Ni islands play an important role to facilitate the growth of MB_6 1D nanostructures.

2. Effect of Catalytic Materials. Controlled experiments of direct pyrolysis of B_2H_6 over MO/SiO_2−Si substrates without introducing any catalytic materials were carried out. No 1D nanostructures could be identified from the substrates after syntheses, indicating the growth of MB_6 1D nanostructures is catalytic materials-assisted. In addition to Ni, other catalytic materials such as gold (Au),

(34) Eitel, W. *Silicate Science, Vol. III, Dry Silicate System*; Academic Press: New York, 1965.
(35) O'Neil, M. J.; Smith, A.; Heckelman, P. E.; Budavari, S. *The Merck Index*; John Wiley & Sons: New York, 2001.
(36) Buffat, P.; Borel, J. P. *Phys. Rev. A* **1976**, *13*, 2287.
(37) Wang, Z. L.; Petroski, J. M.; Green, T. C.; El-Sayed, M. A. *J. Phys. Chem. B* **1998**, *102*, 6145.
(38) Gadkari, P. R.; Warren, A. P.; Todi, R. M.; Petrova, R. V.; Coffey, K. R. *J. Vac. Sci. Technol., A* **2005**, *23*, 1152.
(39) Petersen, J.; Mayr, S. G. *J. Appl. Phys.* **2008**, 103.

platinum (Pt), and palladium (Pd) were employed in experiments. Nickel was found to have the highest catalytic efficiency, followed by Pd, Pt, and Au. This observation is consistent with our previous results.[25,33] Our practices show that, under optimized conditions, (1) Ni catalyzes the growth of MB_6 1D nanostructures, but not boron nanowires; (2) Au has very high catalytic efficiency on growth of boron nanowires, but the lowest efficiency on growth of MB_6 1D nanostructures; and (3) Pt, Pd, and Pt/Pd can catalyze the growth of both MB_6 1D nanostructures and boron nanowires under different growth conditions. For growth of MB_6 1D nanostructures, thickness of the Ni film was varied from 2 to 8 nm. The optimum film thickness for growth of MB_6 1D nanostructures was found to be 2−4 nm. In short, the synthesis of MB_6 1D nanostructures is catalytic materials-assisted, and the optimum growth of these nanostructures requires 2−4 nm Ni.

3. Effect of Substrates. In addition to the typical SiO_2−Si substrates, other substrates such as single crystalline quartz, Si(001), sapphire, and GaN-Al_2O_3 were utilized in this study. For each substrate, MB_6 1D nanostructures similar to those observed from SiO_2−Si substrates were observed, indicating the growth of MB_6 1D nanostructures is substrate-independent.

4. Effect of Reaction Temperatures and Duration. With other parameters (i.e., reaction duration, flow rate, heating and cooling rate, etc.) unchanged, the reaction temperature was varied to 1050 °C. Higher yield of MB_6 1D nanostructures was observed. In addition, controlled experiments on direct heating of MO powders at 1050 °C in the Ar environment revealed larger and more "molten peripheries" compared to those observed from direct heating at 950 °C.

With other parameters (i.e., reaction temperature, flow rate, heating and cooling rate, etc.) unchanged, the reaction duration was varied from 2 to 60 min. The time-dependent morphological evolution of MB_6 1D nanostructures is shown in Figure 5. (i) For nanostructures grown with a shorter reaction time (e.g., 2 min), globes along 1D nanostructures can be identified (Figure 5a,f). TEM/EDX/electron diffraction pattern analyses (Figure 5d,e,i,j) revealed that the globes are amorphous and rich in M, O, and sometimes C, whereas the core 1D nanostructures are single crystalline and rich in M and B. As discussed later in the text, it is believed that the globes were liquid MO droplets at the reaction temperatures and played an important role during the growth of MB_6 1D nanostructures. The presence of C is due to the adsorption of C-containing molecules after exposing the samples to the ambient environment. A relatively larger amount of C can be identified from the BaO globes along the BaB_6 1D nanostructures than that from SrO globes (compare part e of Figure 5 with part j). This is consistent with the reported phenomenon that BaO is the most alkaline among all alkaline-earth metal oxides; it is very alkaline and easily absorbs moisture and CO_2 on exposure to air.[35] (ii) For nanostructures grown with an intermediate reaction time (e.g., 20 min), thicker and longer 1D nanostructures with less globes (indicated by white arrows) were resolved as shown in Figure 5b,g. Moreover, MO solids with irregular shapes can be identified from side surfaces of some 1D nanostructures. As shown in the inset of Figure 5g, flattened solids can be observed from the thicker portion of the 1D nanostructure, whereas spherical-shaped solids can be seen from the thinner portion of the 1D nanostructure. The shape change of the MO solid phases might be related to the diameter-dependent wettability of MO on MB_6. (iii) For the nanostructures grown with a longer reaction time (e.g., 60 min), 1D nanostructures with smoother surfaces can be obtained as shown in Figure 5c,h. In short, time-dependent morphological evolution of MB_6 1D nanostructures were revealed. Results show that longer reaction time can produce single crystalline MB_6 1D nanostructures with smoother surface.

5. Possible Growth Mechanisms. Given that (i) the growth of MB_6 1D nanostructures was catalytic materials-assisted, (ii) catalytic materials were not detected from the tips of nanostructures, (iii) the MO powders were likely in a molten state at the reaction temperatures, and (iv) globes of MO could be observed along the MB_6 1D nanostructures while shorter reaction time was employed, we hypothesize the growth of MB_6 1D nanostructures is dominated by a nontraditional VLS-like growth.[40] This hypothesis involves three main steps.

(1) Melting of the Ni-Coated MO Powders at the Elevated Reaction Temperatures. As discussed above, part of the MO powders is likely in the molten state at the reaction temperatures. Flow of the superficial liquid might also occur, resulting in the formation of "molten peripheries" surrounding the powders on the substrate. The liquid is believed to have a large accommodation coefficient to facilitate the adsorption of borane molecules and the growth of MB_6 1D nanostructures. Although it is not clear which state Ni is in (solid or liquid) at the reaction temperatures, it is believed this catalytic material effectively facilitates the growth of MB_6 1D nanostructures.

(2) Nucleation and Initial Growth of MB_6 1D Nanostructures. The gas-phase chemistry of B_2H_6 pyrolysis is very complex. Various borane molecules can be produced when heating B_2H_6 to different temperatures.[41−44] At lower temperatures, the uncompleted decomposition of B_2H_6 can lead to the formation of several high-order boranes (e.g., B_3H_9, B_4H_{10}, and B_5H_{11}).[41−43] At higher temperatures, the relatively completed decomposition of B_2H_6 can produce BH_3 as the dominant gas-phase species.[42,43] The BH_3 molecules will impinge upon the substrate surfaces and be adsorbed on certain preferred sites. The adsorbed BH_3 molecules can then completely decompose ($2BH_3 \rightarrow B + 3H_2$), producing H_2 gas and leaving boron bonded to surfaces that diffuse into the bulk substrate. In our experiments, the BH_3

(40) Givargizov, E. I. *Highly Anisotropic Crystals*; D. Reidel Publishing Company: Dordrecht, 1987.
(41) Soderlund, M.; Maki-Arvela, P.; Eranen, K.; Salmi, T.; Rahkola, R.; Murzin, D. Y. *Catal. Lett.* **2005**, *105*, 191.
(42) Desrosiers, R. M.; Greve, D. W.; Gellman, A. J. *J. Vac. Sci. Technol., A* **1997**, *15*, 2181.
(43) Lamborn, D. R.; Snyder, D. W.; Xi, X. X.; Redwing, J. M. *J. Cryst. Growth* **2007**, *299*, 358.
(44) Greenwood, N. N.; Earnshaw, A. *Chemistry of Elements*; Reed Educational and Professional Publishing Ltd.: Oxford, U.K., 1997.

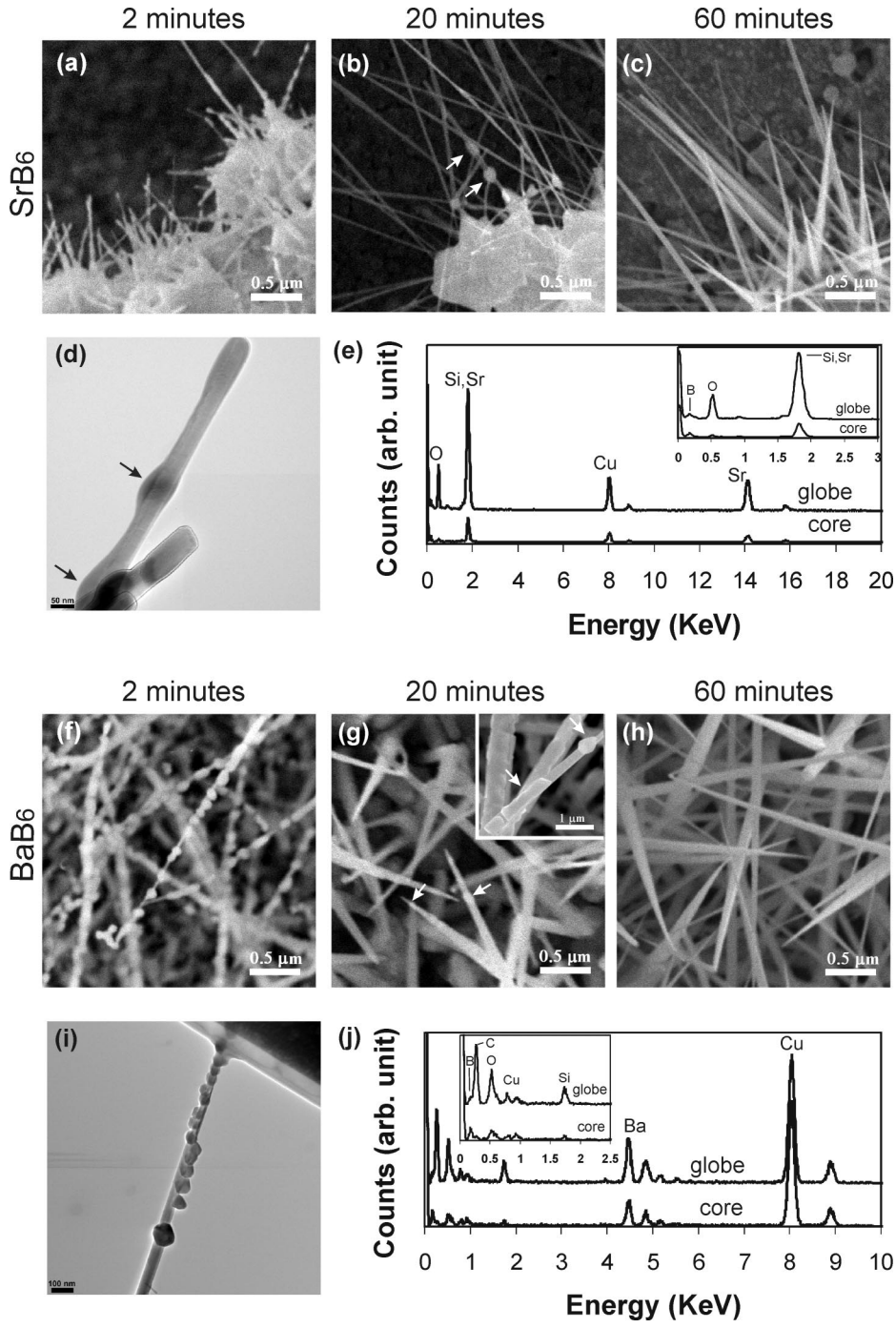

Figure 5. SEM images of reaction time-dependent morphological evolution of SrB_6 (a−c) and BaB_6 (f−h) 1D nanostructures. For MB_6 1D nanostructures grown by shorter reaction time, results disclose the existence of globes along 1D nanostructures. TEM/EDX analyses of SrB_6 (d, e) and BaB_6 (i, j) 1D nanostructures (synthesized by 2 min) revealed the globes are amorphous MO materials, whereas the 1D nanostructures are single crystalline MB_6 materials. The scale bars in parts d and i represent 50 and 100 nm, respectively.

molecules produced by pyrolysis of B_2H_6 at 950 °C could be adsorbed on the MO liquid surface which has a large accommodation coefficient. Afterward, the complete decomposition of BH_3 could produce boron bonded to liquid surface and react with MO to form MB_6 via the chemical reaction of $MO(l) + B \rightarrow MB_6(s) + B_2O_2(g)$. This reaction can be greatly enhanced, and growth of 1D nanostructures can be realized when Ni is introduced and used as the catalytic material. As revealed by X-ray diffraction (results not shown here), very weak peaks corresponding to BaB_6 (100), (111), and (200) were observed from reacted BaO/SiO_2−Si samples where no 1D nanostructures were found. However, stronger peaks were detected from reacted $Ni/BaO/SiO_2$−Si samples where 1D nanostructures as shown in Figure 1 were found. These results imply that Ni can enhance the formation of MB_6 and is necessarily required for the growth of 1D nanostructures. So far, the real mechanisms on how Ni catalyzes the growth of MB_6 1D nanostructures and why Ni does not exist at the tips of 1D nanostructures are not clear. However, it is possible that (1) Ni may lower the barrier that is present for the incorporation of MB_6 at the growth interface (i.e., catalytic material−1D nanostructure interface)

as compared to the nucleation of the MB_6 thin film all over MO or the substrate;[45] and (2) Ni may increase the decomposition efficiency of B_2H_6.[42] Future work such as cross-sectional TEM examination providing more information related to the microstructures surrounding Ni islands and the chemical composition of Ni islands is needed to facilitate a better understanding of this nucleation/initial growth process.

When the MB_6 1D nanostructures nucleated and grew out from the MO liquid, MO droplets or sometimes envelopes could attach on them (see evidence in Figure 5a,f). These MO droplets can then also transform to MB_6 as discussed afterward.

As well-known for the traditional VLS growth mechanism, the existence of catalytic particles at the tips of 1D nanostructures is one of the key characteristics. Although catalytic particles were not detected from the tips of MB_6 1D nanostructures reported here, it is not sufficient to rule out the VLS mechanism.[40] The present growth involves vapor (provided by pyrolysis of diborane), liquid (supplied by melting of MO powders), and solid (realized by formation of MB_6 1D nanostructures). Thus, it can be considered as a "relative" of the classical VLS process as discussed in ref 40 and termed as a nontraditional VLS-like growth. Aforementioned future cross-sectional TEM examination will reveal the role of Ni and provide more insight on the growth mechanism, particularly on whether the 1D nanostructures were grown from their bases or not.

(3) Continuous Growth of MB_6 1D Nanostructures. Continuous exposure to boron-containing vapor species results in (i) nucleation and initial growth of new MB_6 1D nanostructures and elongation of the existing MB_6 1D nanostructures via the aforementioned nontraditional VLS-like growth mechanism and (ii) lateral thickening of MB_6 1D nanostructures. As discussed above, MO droplets could attach along MB_6 1D nanostructures when the nanostructures nucleated and grew out from the MO liquid. The MO droplets could act as new nucleation sites and vapor sinks for lateral growth of MB_6 1D nanostructures. Migration of MO droplets could occur at elevated temperatures. However, when the diameter of 1D nanostructures increased, migrating of MO droplets from roots to tips of the nanostructures became difficult, which in turn could result in the formation of tapered 1D nanostructures.

Conclusion

In summary, SrB_6 and BaB_6 1D nanostructures which are promising low-dimensional thermoelectric materials were synthesized by pyrolysis of diborane over Ni-coated SrO and BaO powders in a home-built LPCVD system. The as-synthesized 1D nanostructures have single crystalline cores and amorphous oxide sheathes. The observation of (i) "molten peripheries" surrounding MO powders and (ii) no catalytic material Ni on the tips of 1D nanostructures suggests that the growth of these MB_6 1D nanostructures might be dominated by a nontraditional VLS-like growth mechanism. Similar results were obtained when $SrCO_3$ and $BaCO_3$ powders were used as solid precursors.

To further understand the growth mechanisms, cast[46] or sputtering deposited uniform MO or MCO_3 thin films will be used as the solid precursor for growth of MB_6 1D nanostructures in future experiments. Cross-sectional TEM examination will be conducted to explore the role of Ni. The better understanding of the growth mechanism will facilitate the high-volume production of MB_6 1D nanostructures for future device application. Measurement of thermoelectric properties of individual 1D nanostructures is currently underway, and special attention will be paid to investigate the effects of amorphous oxide layers.

Note Added in Proof. While this work was under review, a similar work on synthesizing SrB_6 1D nanostructures was published.[47] The differences between their work and ours are (1) our work covered both SrB_6 and BaB_6 1D nanostructures while Jash's work was on only SrB_6 1D nanostructures and (2) a nontraditional VLS-like growth mechanism was identified in our work based on systematic control experiments while a VLS growth mechanism was used to explain the growth of SrB_6 1D nanostructures synthesized by Jash et al.

Acknowledgment. Acknowledgement is made to the Donors of the American Chemical Society Petroleum Research Fund (PRF No. 44245-G10) and National Science Foundation CAREER Award (CMMI 0748090) for partial support of this research. Supports provided by the start-up fund, junior faculty research grant, and Charlotte Research Institute "Wachovia Summer Stipend for New Faculty" at the University of North Carolina at Charlotte (UNC Charlotte) are also appreciated. We are grateful to the RRC facility at the University of Illinois—Chicago for providing the Renishaw Raman spectroscope for the Raman studies, the NU*ANCE* center at Northwestern University for the TEM studies, and the Center for Optoelectronics and Optical Communications at UNC Charlotte for multiuser facilities.

CM802018E

(45) Chen, L. J. *J. Mater. Chem.* **2007**, *17*, 4639.

(46) Solovyov, V. F.; Wiesmann, H. J.; Suenaga, M. *Supercond. Sci. Technol.* **2003**, *16*, L37.

(47) Jash, P.; Nicholls, A. W.; Ruoff, R. S.; Trenary, M. *Nano Lett.* **2008**, *8* (11), 3794.